Graphite intercalation compounds: Electronic properties in the dilute limit*†

M. S. Dresselhaus
Department of Electrical Engineering and Computer Science and Center for Materials Science and Engineering, Massachusetts Institute of Technology, Cambridge, Massachusetts 02139

G. Dresselhaus
Francis Bitter National Magnet Laboratory,§ Massachusetts Institute of Technology, Cambridge, Massachusetts 02139 and Lincoln Laboratory, Massachusetts Institute of Technology,‖ Lexington, Massachusetts 02173

J. E. Fischer
Cavendish Laboratory, Cambridge University, Cambridge, England and Moore School of Electrical Engineering and Laboratory for Research on the Structure of Matter, University of Pennsylvania, Philadelphia, Pennsylvania 19174

(Received 11 October 1976)

A model is presented for the electronic properties of graphite intercalation compounds in the dilute limit, corresponding to intercalate concentrations more dilute than a stage-4 or -5 compound. In this limit, the electronic effect of intercalation in donor and acceptor compounds is modeled, respectively, as a raising or lowering of the Fermi level within the π bands of pure graphite, as represented by the Slonczewski-Weiss-McClure dispersion relations for $E(\vec{k})$. Within this framework we calculate the dependence on Fermi level of the following quantities: (i) the electron and hole carrier densities, (ii) the electron and hole density of states, (iii) the de Haas–van Alphen extremal areas, (iv) the Hall constant in the low-magnetic-field limit, and (v) the in-plane electrical conductivity σ_a, with several different assumptions for the energy dependence of the relaxation time. Distinctive features in the energy dependence for each of these quantities are identified in order to suggest experiments designed to determine the fractional number of carriers introduced per intercalate atom or molecule.

I. INTRODUCTION

Graphite intercalation compounds have been discussed as potentially practical high-conductivity synthetic metals.[1-4] These compounds[1] consist of an alternating sequence of intercalate monolayers separated by n contiguous graphite layers ($n \geq 1$), where n denotes the stage of the compound. The chemical reaction by which the compounds are formed is facilitated by the highly anisotropic bonding in graphite; the hexagonal array within a single carbon layer contains very strong sp^2 covalent bonds, whereas adjacent layers are bonded mainly by the weak p_z overlap between nearest-neighbor layers. As a result, the in-plane graphite structure is essentially unchanged by intercalation, while the c-axis spacing can increase by as much as a factor of 3 to accomodate the intercalate. For higher-stage compounds ($n \geq 2$) the $ABAB$ graphite layer stacking is preserved between the intercalate monolayers.

One of the most striking property changes accompanying intercalation is the large increase in a-axis (in-plane) conductivity σ_a. This property is illustrated by the experimental points in Fig. 1 showing σ_a/σ_a^0 versus concentration x for several intercalate species taken from the work of Ubbelohde and co-workers[2-4]; σ_a^0 denotes σ_a for pure graphite ($x=0$). Because of quantitative discrepancies in the experimental results reported by the same[5] or different[4] workers, the data of Fig. 1 should be considered qualitative. Thus the curves are drawn in Fig. 1 to indicate the general trends of these data. From the signs of the Hall[6] and Seebeck[3,7] coefficients, metallic intercalate species act predominantly as electron donors, whereas acids and halogens behave as acceptors. The increase in σ_a is the net result of changes in free-carrier density and in mobility upon intercalation. The maximum conductivity plotted in Fig. 1, a factor 13 greater than that of pure graphite, is roughly equal to σ of aluminum. Figure 1 implies that the maximum value of σ_a depends primarily on the initial rate of increase, since saturation is observed for most intercalate species.

This initial slope is determined in part by the parameter f, defined here as the fraction of a free hole or electron introduced per intercalate atom or molecule.[8] One is tempted to assume that f is simply related to the difference between the first ionization potential of the intercalate and the work function (or Fermi energy) of graphite.[9] However, no general rules of this kind have emerged, signaling the complex behavior of this highly varied class of compounds. A major motivation of the work reported here was to identify experimentally observable features which may be used to determine f for various intercalate spe-

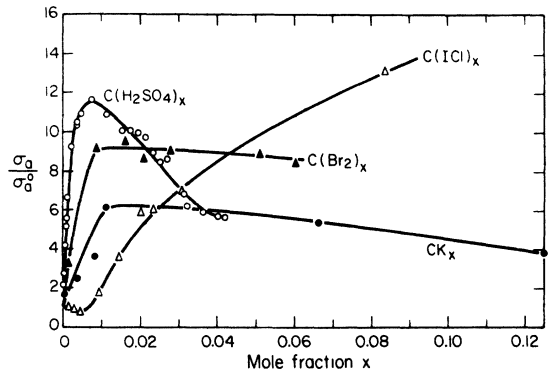

FIG. 1. Dependence on intercalate concentration of the room-temperature in-plane electrical conductivity σ_a of various graphite intercalation compounds normalized to that for pure graphite σ_a^0. The points are the experimental data of Ubbelohde and co-workers (Refs. 2–4) and the curves indicate qualitative trends in these data points. In obtaining the σ_a/σ_a^0 points for CK_x from the R/R_0 data in Ref. 3, corrections were made for the change in the c-axis sample dimensions with intercalation. Mole fractions are computed according to the following chemical formulas for the intercalation compounds: C_8K, $C_{16}(Br_2)$, $C_{12}ICl$, $C_{12}(H_2SO_4)$.

cies, and to provide a theoretical framework for the analysis of such experiments.

Previous work on the transport properties of graphite intercalation compounds has focused on measurement of σ_a versus intercalate concentration and representative curves for such measurements are shown in Fig. 1. For most of the intercalate species shown, σ_a first increases very rapidly with concentration, then saturates or decreases slightly. While all heavy alkali-metal intercalates show identical behavior, the initial slopes shown for the acceptor molecular intercalates Br_2 and H_2SO_4 are quite different from each other and from the initial slope for the donor alkali intercalates. The saturation behavior also differs for the different intercalate species. For the alkali metal and H_2SO_4 intercalate species, saturation is achieved at about a stage 4 compound, but a higher stage is required for the Br_2 intercalate. The observation of this saturation phenomenon for most intercalate species suggests the existence of a dilute limit[10] for low intercalate concentrations, wherein the electronic structure of the compound might be deduced from a rigid-band modification of the graphite electronic structure.

Although the saturation behavior of σ_a versus concentration is typical, it is not universal, as illustrated by the results for ICl where there is no clear evidence for saturation in the published data up to the highest concentration (stage 1 based on the formula $C_{12}ICl$).[11] It should be pointed out that the relation between stage and intercalate concentration x depends on the choice of molecular unit for the intercalate species. Although x-ray data can in principle establish this relation, definitive information is not presently available for the proper molecular units and chemical formulas for many intercalate species (e.g., ICl). Any change in the specification of a molecular unit or chemical formula corresponds to a change in scale in Fig. 1 along the abscissa.

In Sec. II we define and discuss the dilute limit. Section III describes the model used to represent the electronic structure of graphite with Fermi energy E_F as independent variable; results are given for the dependence on E_F of: (a) the densities of electrons and holes $n(E_F)$ and $p(E_F)$, (b) the density of states for electrons and holes $N_e(E_F) \equiv (dn/dE)_{E_F}$ and $N_h(E_F) \equiv (dp/dE)_{E_F}$, (c) the de Haas–van Alphen extremal areas, (d) the in-plane Hall coefficient R_H, and (e) the in-plane electrical conductivity σ_a. In calculating σ_a, several models for carrier relaxation are considered. Plots of $N_e(E_F)$, $N_h(E_F)$, E_F, R_H, and σ_a versus the change in free-carrier density $|n-p|$ are also presented where $|n-p|=0$ for pure graphite. The change in the free-carrier density is useful because it is directly related to the intercalate concentration. Discussion and conclusion are given in Sec. IV.

II. DILUTE LIMIT

The central focus of this work is a discussion of the electronic properties of graphite intercalation compounds in the dilute limit, defined as that range of intercalate concentrations within which the properties can be described by rigid band modifications of graphite. There are several approaches that can be taken to determine the upper bound of the dilute limit and they all lead to essentially the same result; namely, an intercalate concentration corresponding to about a stage 4 or 5 compound, and containing 25–60 carbons per intercalate atom or molecule.

For the compounds showing saturation effects in Fig. 1, the simple behavior of σ_a versus concentration up to about 50 carbon atoms per intercalate atom or molecule suggests that stage 4 or 5 represents the maximum concentration of the dilute limit. This region of simple behavior for various donor and acceptor species suggests a common mechanism for the initial conductivity increase, the magnitude of the initial slope of σ_a being the only property which is specific to a given intercalate.

Another approach to the delineation of the dilute limit is obtained from studies of resonant Landau-level transitions observed in the magnetoreflection

spectra of various intercalation compounds. Although the intensity of the resonances is attenuated with increasing intercalate concentration, it has been possible with present experimental techniques to obtain well-resolved magnetoreflection resonances for concentrations more dilute than about stage 15 for various graphite-halogen intercalation compounds.[12] From analysis of plots of photon energy versus resonant magnetic field (fan charts) for each Landau-level transition, it is found that the magnetic energy-level structure within approximately ± 0.1 eV of the graphite Fermi level is well described by the Slonczewski-Weiss-McClure (SWMcC) band model, using the same order of perturbation theory and approximately the same values of the band parameters as apply to pure graphite.[12-15] These results thus show that well into the dilute region, the energy bands $E(\vec{k})$ near the graphite Fermi level are essentially unchanged by intercalation, thereby suggesting a theoretical model for the discussion of experimental phenomena in dilute graphite intercalation compounds.

An estimate for the dilute limit also follows directly from the SWMcC model.[13,14] Graphite crystallizes in layers perpendicular to the c axis and these layers exhibit an $ABAB\ldots$ stacking arrangement. The electronic structure near the graphite Fermi level is well represented by the SWMcC band model which includes interactions between carbon atoms separated by up to two layer planes. In fact, the band overlap which produces the semimetallic behavior of graphite is associated with the SWMcC band parameter γ_2, representing interactions between atoms two layers apart. Thus, starting from a given graphite layer plane (e.g., an A layer), the smallest unit which would contain the interactions described by γ_2 would be the five layers $ABABA$, corresponding to a stage 5 compound. Thus for $n \gtrsim 5$, larger percentage changes would be expected for γ_2, γ_5, and Δ (representing interactions between carbon atoms two layer planes apart) as compared with the adjacent layer-plane interaction parameters γ_1, γ_3, and γ_4. Furthermore, the nearest-neighbor in-plane overlap integral γ_0 would be expected to show little dependence on intercalate concentration, because the in-plane carbon-carbon bond length is insensitive to intercalation.[16]

An important issue is the extent to which f varies with concentration. For example, one possible explanation for the saturation effect in Fig. 1 is that f decreases as the concentration increases beyond stage 4 or 5, owing perhaps to interactions between intercalate layers separated by fewer than four or five graphite monolayers. The experimental situation is unclear; some authors assume f independent of concentration,[17] while others interpret data in terms of a concentration-dependent f.[3,18] Intuitively one might expect f to be constant within the dilute limit since the intercalate environment is independent of concentration within a sphere of radius > 14 Å encompassing > 80 atoms. This intuitive statement can be experimentally tested for each graphite intercalation compound using the analysis presented here.

Since our dilute limit analysis is based entirely on the electronic properties of pure graphite, we are tacitly assuming that the properties of dilute compounds are dominated by the graphite portion of the crystal. This seems reasonable for most properties, with an obvious exception of c-axis transport. For example, even if intercalate and carbon atoms contribute equally to $N(E_F)$, a calculation which accounts only for the graphite bands will err by 5% at most (e.g., in the stage 4 compound $C_{24}H_2SO_4$). Moreover, the electronic interaction between graphite and intercalate layers is localized close to the intercalate monolayer positions so that in the dilute limit most of the graphite layers are essentially unaffected by the presence of the intercalate. Because of the unusually large basal plane mobility in graphite compared to that of the intercalate species in their crystalline phases, the major contribution to σ_a in dilute compounds is expected to come from the graphite layers.

In our treatment, the dilute region spans the range of stages $\infty > n > 4-5$, corresponding to at least 48–60 (carbon atoms)/(intercalate atom) for the heavy alkali intercalate species or to 24–30 (carbon atoms)/(intercalate molecule) for HNO_3 or H_2SO_4. Differences in mole fraction for different species result from the variety of intercalate molecular units and molecular arrangements that are found in the intercalate monolayers.

III. MODEL AND RESULTS

Transport and Fermi-surface measurements provide information on both the magnitude of f and its dependence on intercalate concentration. Because transport properties depend on both carrier mobility, it is useful to examine various transport and Fermi-surface measurement techniques to determine how they might be interpreted to provide information on f. To this end, we use a modification of the SWMcC band model to calculate the dependence on Fermi level E_F of the carrier density, the density of states, the de Haas–van Alphen extremal areas, the electrical conductivity, and the Hall effect for graphite intercalation compounds in the dilute limit. We assume that the introduction of acceptors corresponds to a lower-

ing of E_F while donor intercalation corresponds to a raising of E_F.

In pure graphite the electron and hole pockets are located along the HKH edges of the Brillouin zone as shown in Fig. 2.[15] The introduction of acceptors increases the volume enclosed by the hole Fermi surface and correspondingly decreases the volume within the electron Fermi surface, while the introduction of donors produces the opposite effect. The energy bands which define the electron and hole Fermi surfaces are shown in Fig. 3. The central panel shows $E(\vec{k})$ along the k_z direction parallel to the c axis, expressed in terms of the dimensionless variable $\xi = ck_z/2\pi$. Here it is seen that the E_3 bands, which are doubly degenerate along the Brillouin-zone edge, define the majority electron- and hole-carrier pockets while the E_1 and E_2 bands play a role in defining the minority hole or electron pockets. In the left-hand panel, the lifting of the degeneracy of the E_3 bands is shown as a function of the dimensionless wave vector σ measured perpendicularly from the K point on the zone edge HKH. The right-hand panel shows the corresponding dispersion curves about the zone corner (H point). These diagrams neglect the trigonal warping of the Fermi surface ($\gamma_3 = 0$). In the present calculation we also neglect trigonal warping in order to simplify the calculation. At least near E_F^0 (the Fermi level for pure graphite), γ_3 has a relatively small effect on the volumes enclosed by the constant energy surfaces. Since the effect of γ_3 is more pronounced near the K point and is negligible near the H point, trigonal warping is expected to be more important for calculating the transport properties associated with electrons. Trigonal warping would be expected to have a large effect on the Fermi surface in the vicinity of the crossing of the E_3 levels through E_F. In fact, for acceptor intercalation compounds, trigonal warping effects could result in the emergence of new pieces of Fermi surface. By using numerical integration techniques the present calculation could be refined to include the effects of trigonal warping.

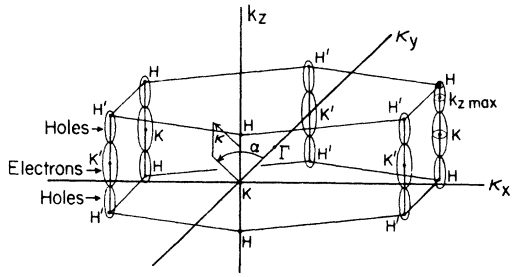

FIG. 2. Graphite Brillouin zone showing schematically the location of the electron and hole Fermi surfaces in pure graphite or in the dilute graphite intercalation compounds in the two-carrier regime. Also shown are the extremal cross-sectional areas for majority electrons about the K point, for majority holes about the $k_{z\,max}$ point, and for minority holes about the H point.

In the present calculation the SWMcC parameter Δ which represents the difference in potential energy between carbon atoms on A and B sites was taken to be negative in accordance with recent H-point magnetoreflection results.[19] Since intercalation disturbs the $ABAB$ stacking of the graphite layers, the magnitude of Δ would be expected to decrease upon intercalation. But since the magnitude of Δ is already so small, it would be difficult to measure the dependence of Δ on intercalate concentration.

The present calculation is similar to the Ono and Sugihara theory of transport properties in pure graphite[20] except for the following two aspects. In the present work there is a different identification of electron and hole pockets in the Brillouin zone.[21] Whereas the temperature dependence of the transport properties in pure graphite is stressed in the work of Ono and Sugihara, the present work focuses on the effect of variation of the Fermi level on these transport properties.

Using the SWMcC band model as described above, the dependence of the electron carrier density $n(E_F)$ on Fermi level E_F is expressed by the relation

$$n(E_F) = (2/4\pi^3)V_e(E_F)\,, \tag{1}$$

where $V_e(E_F)$ is the volume enclosed by the electron constant-energy surface at energy E_F, mea-

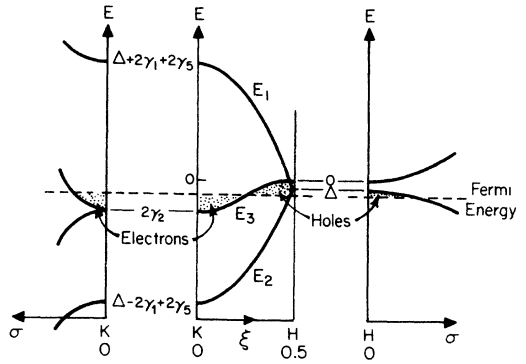

FIG. 3. Wave-vector dependence of the four π-band energy levels according to the SWMcC band model. Left-hand panel shows $E(\sigma)$ about the K point in the Brillouin zone where σ is the dimensionless wave vector in the layer plane. Central panel shows $E(\xi)$ along the Brillouin zone edge HKH in terms of the dimensionless wave vector ξ for $\Delta < 0$. Right panel shows $E(\sigma)$ vs σ about the H point in the Brillouin zone.

sured relative to the zero of energy taken as the energy of the E_3 levels at the H point. (See Fig. 3.) A factor of 2 has been inserted to account for the two full electron ellipsoids which are contained within the Brillouin zone shown in Fig. 2. For the case of both electrons and holes, the volume $V(E_F)$ is found by integrating the cross-sectional Fermi-surface area $A(k_z, E_F)$ over the variable k_z. If γ_3 is neglected, this cross-sectional area is circular and the expression for $A_e(k_z, E_F)$ for electrons is given by the SWMcC model as[14,20,21]

$$A_e(k_z, E_F) = \frac{4\pi}{3a_0^2\gamma_0^2} \frac{1}{(1+\nu)^2} (E_2 - E_F)(E_3 - E_F) . \tag{2}$$

Here a_0 and c_0 are the lattice constants $a_0 = 2.46$ Å and $c_0 = 6.74$ Å,

$$\nu = 2(\gamma_4/\gamma_0) \cos \tfrac{1}{2} c_0 k_z , \tag{3}$$

$$E_2 = \Delta - \gamma_1 \Gamma + \tfrac{1}{2} \gamma_5 \Gamma^2 , \tag{4}$$

$$E_3 = \tfrac{1}{2} \gamma_2 \Gamma^2 , \tag{5}$$

in which

$$\Gamma = 2 \cos \tfrac{1}{2} c_0 k_z \tag{6}$$

and γ_0, γ_1, γ_2, γ_4, γ_5, and Δ are band parameters of the SWMcC band model.[12-15] The volume enclosed by the hole Fermi surface is found in a similar way by a k_z integration of the cross-sectional area for the hole pockets $A_h(k_z, E_F)$ where

$$A_h(k_z, E_F) = \frac{4\pi}{3a_0^2\gamma_0^2} \frac{1}{(1-\nu)^2} (E_1 - E_F)(E_3 - E_F) , \tag{7}$$

in which

$$E_1 = \Delta + \gamma_1 \Gamma + \tfrac{1}{2} \gamma_5 \Gamma^2 \tag{8}$$

and the other quantities are defined above. The k_z integration of $A(k_z, E_F)$ can be carried out analytically resulting in volumes for electrons and holes $V_e(E_F)$ and $V_h(E_F)$. Thus analytic expressions can be obtained for the electron and hole concentrations $n(E_F)$ and $p(E_F)$ at energy E_F. In turn, differentiation with respect to E provides analytic expressions for the density of states $N_e(E) \equiv dn(E)/dE$ and $N_h(E) \equiv dp(E)/dE$. It should be noted that this calculation is appropriate for low temperatures where the thermal carrier excitation is negligible compared with the intrinsic carrier concentration enclosed by the Fermi surfaces.

The values of the SWMcC band parameters in the present calculation (see Table I) are chosen to provide a good fit to the K- point and H-point magnetoreflection spectra, as well as to the majority and minority de Haas–van Alphen periods.[15,21] Using these values for the SWMcC parameters we have plotted in Fig. 4 the carrier densities for the cases $\gamma_4 = 0$ (dashed curve), corresponding to equal effective masses for the valence and conduction E_3 bands and $\gamma_4 = 0.12$ eV (solid curve), corresponding to the experimentally determined values for these masses. Most calculations of transport properties in graphite are for simplicity made with $\gamma_4 = 0$. Since γ_4 is related to the difference between valence- and conduction-band masses,[21] the best available value for γ_4 was used in the present work because of our interest in establishing differences between electron and hole states which arise from the band structure. Note that the curves for $\gamma_4 = 0$ are quite symmetrical under interchange of electrons and holes. This symmetry is reduced by the introduction of nonvanishing values of γ_4. Magnetoreflection data[12] show that, within experimental error, γ_4 does not depend on intercalate concentration x for x less than about a stage 15 compound.

Note that the electron density is zero for hole

TABLE I. Parameters of the SWMcC band model used in the calculations reported here. Except for γ_3, these values are the best available from experiments (Refs. 12, 15, 21). The approximation $\gamma_3 = 0$ gives closed-form solutions for the quantities of interest (see text).

SWMcC band parameters	Values (eV)
γ_0	3.12
γ_1	0.377
γ_2	−0.0206
γ_3	0
γ_4	0.120
γ_5	0.025
Δ	−0.009

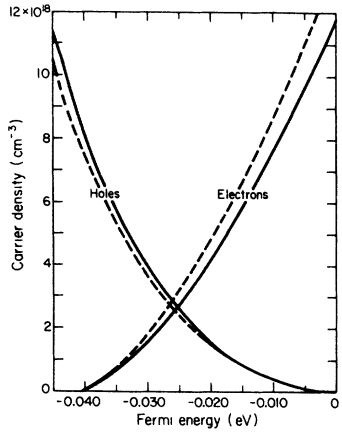

FIG. 4. Fermi-level dependence of the electron- and hole-carrier densities for values of the SWMcC band parameters given in Table I. Solid curves are for $\gamma_4 = 0.120$ eV while the dashed curves are for $\gamma_4 = 0$.

densities greater than $8.8\times10^{18}/\mathrm{cm}^3$; this occurs when E_F decreases to lie below the E_3 band extremum at the K point (see Fig. 3), producing a one-carrier hole system. Similarly when $n>1.2\times10^{19}/\mathrm{cm}^3$ in Fig. 4, a one-carrier electron surface results from the increase of E_F to lie above the H-point extremum of E_3 (Fig. 3). All numerical results presented in this paper include contributions from both majority and minority electrons and holes.

Many transport properties depend on the density of states. The density of states curves corresponding to $n(E_F)$ and $p(E_F)$ of Fig. 4 are plotted in Fig. 5. Of significance is the difference in magnitude between $N_e(E_F)$ and $N_h(E_F)$, and the discontinuities in $N_h(E_F)$ and $N_e(E_F)$ as E_F crosses the K- and H-point extrema of the E_3 bands, respectively (see Figs. 3 and 4). Therefore a transport or specific-heat measurement which is sensitive to the density of states can be used to determine these critical energies E_F^x.

To facilitate contact with the intercalation problem, we consider the excess carrier density of either holes or electrons which can be expressed as $|n-p|$. In the dilute limit, the excess carrier density $|n-p|$ is expected to vary monotonically with intercalate concentration x, noting that in the two carrier regime the addition of acceptor (donor) intercalate species both increases the hole (electron) concentration and decreases the electron (hole) concentration. From Figs. 4 and 5, we can relate E_F to n (or p) and to $N(E_F)$. Subtracting $n-p$, we plot in Fig. 6, $N_h(E_F)$ vs $p-n$, appropriate to acceptor intercalation and $N_e(E_F)$ vs $n-p$ corresponding to the donor case. The singularities in $N(E_F)$ occur at the transition from two- to one-carrier behavior; this transition occurs when E_F crosses the E_3 band K- and H-point extrema. Assuming that f is independent of intercalate concentration, a measurement of $N(E_F)$ versus concentration can be scaled directly along the abscissa of Fig. 6, the scale factor being f. Independent of any concentration dependence that f might exhibit, the discontinuities in $N(E_F)$ provide an attractive possibility for interpreting specific-heat data to yield a value for f at E_F^x, although it may be difficult to extract experimentally an accurate linear specific-heat term with so small a density of states, $N(E_F)\sim5\times10^{20}/\mathrm{cm}^3\cdot\mathrm{eV}$. It is of interest to observe that in the region of E_F^x the density of states for holes is considerably greater than that for electrons. Thus for the same excess carrier density, a dilute acceptor compound would tend to result in a higher conductivity than a dilute donor compound.

Also plotted in Fig. 6 as a function of $|n-p|$ is the shift in Fermi level $\Delta E_F=|E_F-E_F^0|$ relative to that in pure graphite. The range of abscissa values in Fig. 6 corresponds to Fermi level shifts ΔE_F comparable with the graphite π-bandwidth at the K point; for large ΔE_F values there is significant population of the E_1 and E_2 bands (e.g., for $|\Delta E_F|\cong0.3$ eV, 10% of the carriers are associated with the E_1 and E_2 bands).

The upper abscissa in Fig. 6 specifies the intercalate concentration corresponding to the carrier density on the lower scale assuming that $f=1$. The

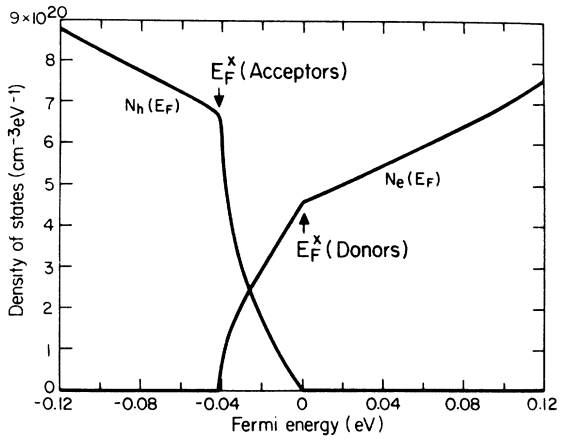

FIG. 5. Fermi-level dependence of the density of states $N_e(E_F)$ and $N_h(E_F)$ for electrons and holes. Singularities of these curves, labeled E_F^x, correspond to the passage of the Fermi level through the K and H point E_3-band extrema.

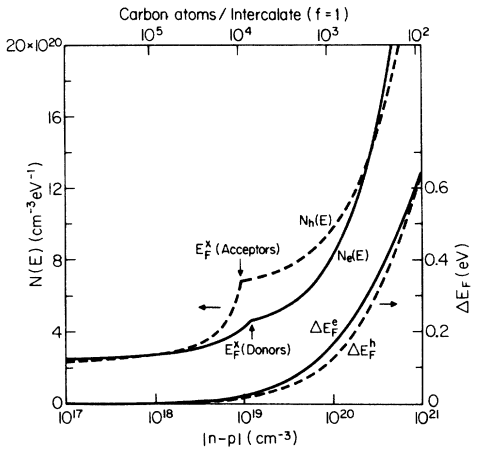

FIG. 6. Hole and electron density of states vs the change in carrier density $|n-p|$ for pure graphite. Also plotted is the corresponding change in Fermi level $\Delta E_F=|E_F-E_F^0|$ where E_F^0 is the Fermi level for pure graphite. On the upper scale the number of carbon atoms per intercalate atom or molecule corresponding to $|n-p|$ is given, assuming unit charge transfer ($f=1$). The locations of E_F^x for acceptors and donors are also indicated (see text).

highest concentration on Fig. 6, $10^{21}/cm^3$, corresponds to 113 carbon atoms per intercalate atom or molecule which in turn corresponds to stage 9 for the heavy alkalis or to stage 18 for certain acceptors, well within the dilute limit. If $f<1$ a larger intercalate concentration would be required to achieve a given $|n-p|$; thus the upper scale would correspond to fewer carbon atoms per intercalate atom or molecule and hence to a lower stage. If $f \ll 1$, the highest concentrations in Fig. 6 may exceed the theoretically defined dilute limit.

On the basis of Eqs. (2) and (7) of the SWMcC model, the dependence of the Fermi-surface extremal cross-sectional areas on Fermi energy can be calculated. Results for the electron and hole extremal cross-sectional areas are given in Fig. 7. For $E_F - E_F^0 > -0.015$ eV, E_F lies above the E_3 band extremum at the K point, giving rise to an electron pocket with an extremal in-plane cross-sectional area passing through the K point ($\xi = 0$). For this carrier pocket the extremal area always passes through the K point, independent of the position of E_F. When E_F falls below the K-point E_3 band extremum, a hole surface forms; in this case also, the hole extremal cross-sectional area passes through the K point. Results for the electron ($E_F - E_F^0 > 0.015$ eV) and hole ($E_F - E_F^0 < 0.015$ eV) extremal cross-sectional areas about the K point are shown in Fig. 7.

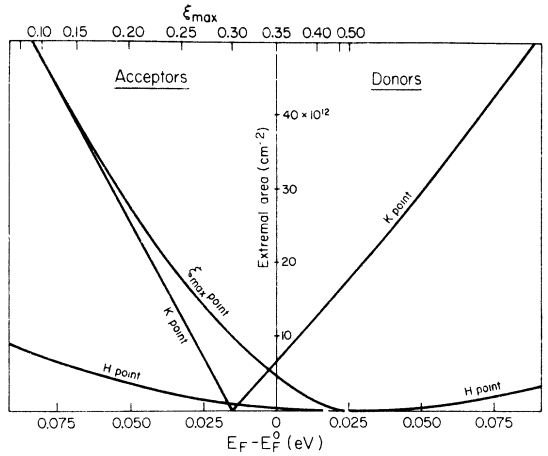

FIG. 7. Extremal Fermi-surface cross-sectional areas for the majority and minority electron and hole pockets (see Fig. 2) vs the change in Fermi energy $E_F - E_F^0$ as produced by acceptor and donor intercalation. By symmetry, the planes through the H and K points and perpendicular to the k axis always yield extremal cross-sectional areas. There is an additional extremal area associated with the holes (labeled ξ_{max} point) occurring at $\xi = \xi_{max}$ and the values for ξ_{max} corresponding to these extremal areas are given by the upper abscissa scale. Particular choice of band parameters (Table I) results in no H point periods in the region $0.016 < E_F - E_F^0 < 0.025$ eV.

In contrast with the Fermi surface evolving from the majority electron surface described above, the Fermi surface which evolves from the majority hole surface has the location of its extremal cross-sectional area (denoted by ξ_{max}) dependent on the position of E_F. Results for this extremal area versus $E_F - E_F^0$ are presented in Fig. 7 on the curve labeled ξ_{max} point. The dependence of ξ_{max} itself on E_F is shown on the upper abscissa scale of Fig. 7, and we note that for $E_F = E_F^0$, $\xi_{max} = 0.35$. As E_F is lowered, ξ_{max} increases until $\xi_{max} \to 0.5$ (about the H point) where the majority hole surface disappears; here E_F crosses the H-point E_3-band extremum.

In addition, minority electron and minority hole Fermi surfaces are found with extremal cross-sectional areas around the H point. For pure graphite the minority pocket is a *hole* pocket. This pocket grows in size as E_F is lowered, but decreases in size as E_F is raised. The minority hole surface disappears when E_F crosses the H point degenerate E_1, E_2-band extremum. On the other hand, the minority electron surface about the H point emerges when the Fermi level is raised above the H-point E_3-band extremum as shown in Fig. 7.

The results for the dependence of the extremal cross-sectional Fermi-surface areas on Fermi level can be applied to the interpretation of the concentration dependence of quantum oscillation periods. Such an analysis could provide an estimate for f and possibly some information on the dependence of f on intercalate concentration. Bender and Young[22] measured the Shubnikov–de Haas periods for various dilute graphite-Br_2 compounds. These authors interpreted their data using a model in which the intercalated planes are Br^- ions (i.e., $f = 1$) and for this reason did not measure the intercalate concentration corresponding to the observed Shubnikov–de Haas periods. According to their interpretation, they identified the observed periods in the intercalation compounds with slightly shifted pure graphite periods and additional short periods (large cross-sectional areas) associated with those graphite planes adjacent to the intercalate layer. Thus their experiments on intercalated single-crystal graphite are consistent with their model of a multiphase compound with complete dissociation and ionization of the Br_2. Other experiments[12] suggest that a single-phase material should exist under the sample preparation conditions used by Bender and Young. If their samples are indeed well-ordered and single-phase, then the observed hole period is only slightly shifted from that of pure

graphite so that their Shubnikov–de Haas data could also be interpreted in terms of a model of molecular intercalation with a very small value for f.[23] Recent de Haas–van Alphen experiments on dilute graphite-Br_2 compounds[24] are also consistent with either multiphase graphite-Br_2 samples or a very small value of f. The observed new short periods[22] could possibly be identified with large breakthrough orbits introduced by the change of periodicity resulting from intercalation.

The SWMcC model can also be used as the basis for a calculation of the magnetoconductivity tensor,[20,25] thereby yielding the dependence of the in-plane electrical conductivity σ_a and Hall constant R_H on Fermi level. The following simplifying assumptions are made: (a) the low-temperature limit is taken so that the Fermi distribution is a step function; (b) the relaxation time for a given E_F value is assumed to be independent of wave vector on the Fermi surface. (Several models for the energy dependence of τ have been considered and are discussed below.) (c) The low magnetic field limit is taken ($\omega_c\tau \ll 1$) so that only the linear term in magnetic field need be considered in calculating the Hall constant R_H; (d) as above, trigonal warping of the Fermi surface is neglected ($\gamma_3 = 0$), greatly simplifying the analytic expressions for the cross-sectional Fermi-surface areas. A generalization could be made to include the effect of γ_3 and of finite temperature in the distribution function. Such refinements would be motivated by the availability of more accurate experimental data. The present calculation is intended merely to serve as a guide for the interpretation of currently available data and as a stimulation for new measurements.

The following geometrical arrangement was used in the calculation. A constant magnetic field was taken along the c axis ($\hat{z}$ direction), constant current in the $\hat{x}$ direction, and Hall probes in the $\hat{y}$ direction, so that the $\hat{x}$ and $\hat{y}$ directions lie in the layer planes. The conductivity tensor has an in-plane diagonal component ($\sigma_{xx} = \sigma_a$) given by

$$\sigma_{xx} = \frac{e^2}{4\pi^3} \int \tau v_\rho^{\,2} \frac{dS}{|\nabla_k E|} , \tag{9}$$

in which τ, the relaxation time, is assumed independent of carrier type. The in-plane velocity component v_ρ in Eq. (9) is obtained from the energy dispersion relations by $v_\rho = \partial E/\hbar\partial k_\rho$, $|\nabla_k E|$ is the gradient of the electronic dispersion relation, and dS is the differential area on the constant energy surface at energy E. By taking $\gamma_3 = 0$, there is no angular dependence of the integrand and an explicit integration need only be performed as a function of k_z. This integration is over electron, hole, and minority carrier constant energy surfaces. The c-axis conductivity σ_{zz} is obtained from Eq. (9) upon substitution of z for x, and v_z for v_ρ.

The off-diagonal conductivity tensor σ_{xy} is given by

$$\sigma_{xy} = \frac{e^2}{4\pi^3} \int \tau^2 \omega_c v_\rho^{\,2} \frac{dS}{|\nabla_k E|} , \tag{10}$$

where the cyclotron frequency $\omega_c = eH/m_c^* c$ is a function of energy and of k_z, but has no angular dependence when γ_3 is neglected.

The Hall coefficient R_H is related to the conductivity tensor components by

$$R_H = -(\sigma_{xy}/\sigma_{xx}^2 H) \tag{11}$$

and for the assumptions made here R_H is independent of relaxation time τ in the low magnetic field limit. A plot of the Hall coefficient versus Fermi energy is shown in Fig. 8. Here the curves for R_H labeled "electrons" and "holes" correspond, respectively to the raising and lowering of the Fermi level. Both curves exhibit two-carrier behavior when E_F is between the H- and K-point E_3-band extrema. A nonvanishing Hall constant is found at the Fermi level for pure graphite $E_F^0 = -0.025$ eV because the holes have a higher mobility than the electrons, in agreement with low-temperature experimental results.[15] Furthermore, within the two-carrier region a sign reversal in R_H occurs when a transition is made from dominance from one carrier type to the other. In both the one-

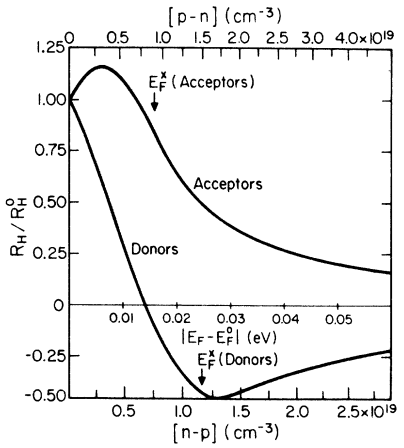

FIG. 8. Calculated Hall coefficient relative to that for pure graphite vs absolute value of the energy difference from the Fermi energy for pure graphite. Curve marked "donors" corresponds to raising the Fermi energy, whereas the curve marked "acceptors" corresponds to lowering the Fermi energy. Both curves exhibit two carrier effects in the band overlap region. On the lower (upper) scale, the change in carrier density $|n-p|$ corresponding to $|E_F - E_F^0|$ is given. Locations of E_F^x are also indicated (see text).

carrier electron region and the one-carrier hole region, R_H is inversely proportional to the electron and hole carrier densities, respectively. The transition from the one- to two-carrier regimes occurs when the Fermi level crosses the H- and K-point E_3-band extrema at E_F. An identification of the extrema in R_H with the Fermi-level crossings is, however, approximate because R_H not only depends on carrier density but also to some extent on the relative mobilities of holes and electrons and on the model assumed for the relaxation time. Nevertheless, inspection of the experimental dependence on intercalate concentration of the extrema in R_H can be used to *estimate* f, particularly for donor compounds. Furthermore, in the one-carrier regime, measurement of R_H in the low-field limit can be used to obtain f directly for any intercalate concentration. To facilitate comparison with experiment, the excess carrier concentration $(p-n)$ for the hole curve is given on the upper abscissa scale, and $(n-p)$ for the electron curve is given on the lower abscissa scale. Note that the critical energy is acheived with ~25% fewer acceptors than donors, another manifestation of the asymmetry between $N_e(E)$ and $N_h(E)$ discussed earlier.

If the carrier densities can be determined (at least approximately) from Hall measurements, then the electrical conductivity can be used to provide information on the carrier mobilities. The carrier mobility depends both on the carrier effective mass and on τ. For the ordered intercalation compounds, there should be *no* contribution to carrier scattering from a disorder or charged impurity mechanism. However, an increased scattering rate would result from the increase in the density of states at the Fermi level or possibly from new umklapp processes due to zone folding.

To study the E_F dependence of the effective mass contribution to τ, the dependence of σ_a on E_F was calculated assuming τ to be independent of E_F and k_z (τ = constant model). The σ_a results for donor and acceptor compounds (raising and lowering E_F) are shown in Fig. 9 (dashed curves) in which E_F is expressed relative to E_F^0 for pure graphite. For the constant τ approximation σ_a is a monotonically increasing function of E_F. For example, lowering (or raising) E_F by ~0.15 eV increases σ_a by an order of magnitude; however, for the same nominal change in E_F, the increase in σ_a is somewhat greater for the case of acceptors than for donors.

A physical mechanism that roughly corresponds to an energy-independent τ is small-angle grain-boundary scattering within the graphite layer planes. This mechanism would be more accurately described by an energy-independent mean-

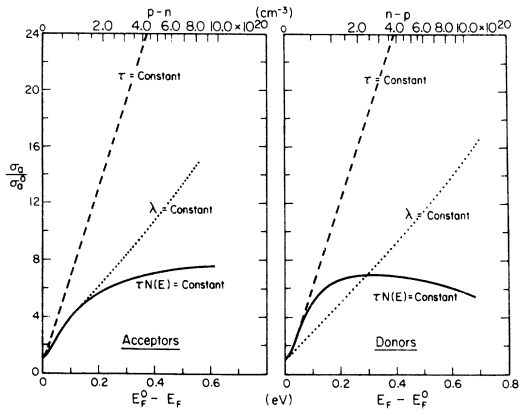

FIG. 9. Calculated in-plane electrical conductivity σ_a relative to that for pure graphite σ_a^0 vs $|E_F - E_F^0|$. The curves marked "*acceptors*" and "*donors*" correspond, respectively, to the lowering and raising of the Fermi level. Three scattering mechanisms are an energy-independent relaxation time τ = constant (dashed curve), a constant electron mean free path λ = constant (dotted curve), and τ inversely proportional to the density of states at the Fermi level [solid curve labeled $\tau N(E)$ = constant]. Upper scales give the change in carrier density $|n-p|$ corresponding to $|E - E_F^0|$.

free path λ, and results for the dependence of σ_a on E_F for a constant λ are also shown in Fig. 9 (dotted curve) for comparison. In calculating σ_a for λ = constant, the integration in Eq. (9) is carried out for $\lambda = \tau v_\rho$, independent of E_F and k_z. The results for the λ = constant approximation (see Fig. 9) again show σ_a to be a monotonically increasing function of $E_F - E_F^0$ but having a smaller slope than for the τ = constant model, so that to produce an order of magnitude change in σ_a a larger change in E_F (~0.4 eV) is required. Thus the interpretation of experimental σ_a data by the τ = constant model would yield a smaller value for f than by the λ = constant model.

The most probable scattering mechanism except at very low temperature is by phonons, and would involve scattering to an arbitrary point on the Fermi surface. We model this scattering process by assuming an energy-independent electron-phonon scattering cross section and thus $1/\tau$ can be assumed proportional to the density of states $N(E)$ at the Fermi surface. The phonon scattering mechanism would be expected to be more important at high temperatures because of the unavailability of large wave-vector phonons at low temperatures. Results for the energy dependence of σ_a for the model $\tau N(E_F)$ = constant are shown in Fig. 9 (solid curve). For both donor and acceptor compounds, these curves show an initial rapid rise in σ_a for changes in E_F up to about 0.1 eV, followed by saturation at about $7\sigma_a^0$, where σ_a^0

corresponds to pure graphite. The rapid rise in σ_a is associated with the region in Fig. 6 where $N(E_F)$ has a weak dependence on carrier density and therefore τ is only weakly dependent on E_F. Far from E_F^0, the integral in Eq. (9) is essentially proportional to the density of states, so the phonon scattering mechanism eventually results in a saturation in σ_a. The detailed energy dependence of σ_a in the saturation region is different for electrons and holes, with the electron curve showing a slow decrease in σ_a at high $E_F - E_F^0$ values, which is not present in the hole curve. Since the conductivity σ_a is normalized to σ_a^0 for pure graphite, no adjustable parameters are used to calculate σ_a/σ_a^0.

To facilitate the comparison of these curves to experimental σ_a data, plots of σ_a/σ_a^0 vs. $p-n$ and $n-p$ are presented in Fig. 9, using the upper abscissa scale. It is of interest that the scattering mechanisms considered here yield both a monotonic increase in σ_a/σ_a^0 (ICl) and a saturation effect (other intercalate species in Fig. 1). By considering the scattering rate to be due to one or more scattering mechanisms, these calculated σ_a/σ_a^0 curves can be fit to experimental data to determine f. In combination with Hall effect measurements on the same samples, an analysis of R_H and σ_a data could also provide information on the scattering mechanism for various intercalate species. An example of the fitting of Fig. 9 to experimental data will be given in the next section.

IV. DISCUSSION

The central focus of this discussion is the application of the calculations of Sec. III to experimental data in an attempt to infer the free carrier concentrations introduced by a given intercalate concentration. In comparing the results in Sec. III with experimental data, caution should be exercised for the following reasons: (a) the present calculation is only applicable in the dilute limit whereas most experimental data emphasize the higher concentration range; (b) the calculation is appropriate to low temperatures while most published experimental data are for room temperature; (c) the calculation neglects possible contributions to the transport properties from the intercalate monolayers.

The distinctive features in the E_F dependence of the electron and hole carrier concentrations shown in Fig. 4 and of the electron and hole density of states shown in Fig. 5 are associated with the passage of E_F through the K- and H-point E_3-band extrema. Since no singularities in the electron and hole carrier concentrations appear at the electron and hole cutoff energies, measurements which focus primarily on $n(E)$ and $p(E)$ are not promising for identifying the passage of the Fermi level through the K- and H-point E_3- band extrema. On the other hand, singularities *are* found in the density of states curves $N_e(E)$ and $N_h(E)$ at these critical Fermi-level positions (see Fig. 5). Therefore measurements such as the determination of the electronic specific heat could be used to identify these critical energies, thereby yielding a direct determination of f.

A comparison between the observed de Haas–van Alphen extremal cross-sectional areas versus intercalate concentration with the calculated curves in Fig. 7 versus $|n-p|$ could be interpreted to yield both the magnitude of f and any possible variation with intercalate concentration for the very dilute range where the de Haas–van Alphen effect can be observed. In this very dilute range, the de Haas–van Alphen effect provides a very sensitive method for the determination of f. On the other hand, the Shubnikov–de Haas data reported by Bender and Young[22] cannot be used to yield an explicit value for f because the intercalate concentration for the various samples was not measured directly. Furthermore, the observed change in the majority hole period was so small that all that can be concluded from these data is that f for graphite-Br_2 is very small, consistent with the interpretation of other measurements.[23]

The interpretation of Hall data also provide a sensitive measure for f. The passage of E_F through the E_3-band extrema corresponds to the transition from two- to single-carrier conduction, and gives rise to the extrema in the E_F dependence of R_H, as shown in Fig. 8. These distinctive extrema do not exactly coincide with transitions from two- to single-carrier conduction regimes because R_H for a two-carrier system depends on both carrier density and mobility and because R_H is somewhat sensitive to the approximation used for the E_F dependence of τ. To identify these distinctive features, low-temperature R_H data should be used so that carrier generation by the intercalate species dominates the thermal generation. At higher intercalate concentrations corresponding to the one-carrier regime, measurement of R_H directly determines the carrier density, thereby yielding both f and its dependence on intercalate concentration. However, if the intercalate species should contribute to conduction, such contributions could introduce errors in the use of Hall data to determine the carrier density in the graphite layers. It should be emphasized that low-temperature (77 K) Hall measurements in the transition region to one-carrier behavior and in the one-carrier regimes provide a powerful tool for the study of f.

The distinctive features of the energy dependence of the in-plane electrical conductivity curves (Fig.

9) are the slope of the monotonically increasing region and the transition from the monotonically increasing region to the saturation region. These features also appear in the experimental (σ_a/σ_a^0) data for most of the intercalate species that are shown in Fig. 1, although the experimental and theoretical saturation phenomena should not be compared directly since the former is outside the scope of the dilute limit. Because of the sensitivity of the initial slope to the scattering model, use of the initial slope data is not attractive for the determination of f at present, since the scattering processes in graphite intercalation compounds have not been studied extensively to date; thus one has little guidance as to the correct scattering mechanism. On the other hand, the saturation behavior predicted for σ_a/σ_a^0 vs $E_F - E_F^0$ with donor intercalation is suggestive of the observed σ_a/σ_a^0 vs x, the intercalate concentration dependence for alkali metals. In Fig. 9, the maximum σ_a/σ_a^0 for electrons occurs at $\Delta E_F \sim 0.2$ eV, which, according to Fig. 6, corresponds to approximately the formula $C_{800}M$ (where C denotes a carbon atom and M denotes an intercalate atom or molecule), which in turn corresponds approximately to a stage 60 compound assuming $f = 1$. Experimentally the maximum is found at $\sim C_{50}M$ or stage 5 (Fig. 1). This would imply $f \ll 1$ for the alkali metals, in contrast to the value[26] $f = 0.75$ obtained from analysis of Hall data for the stage 3 compound $C_{36}Cs$. Therefore the similarities between the $\tau N(E) =$ constant curves in Fig. 9 and the data of Fig. 1 may be more accidental than real; as stated earlier, other observables such as $N(E_F)$, R_H, and the de Haas–van Alphen periods which either are independent of or relatively insensitive to assumptions for τ, are preferable to σ_a for the determination of f by comparison between calculation and experiment.

Normalization of σ_a for an intercalation compound to σ_a^0 for pure graphite reduces the sensitivity of the in-plane conductivity to the relaxation time. It is for this reason that the results in Fig. 9 are presented in terms of σ_a/σ_a^0. For each scattering mechanism considered in Fig. 9, there are no adjustable parameters required to match ordinates. For a real material, the scattering may in fact include more than one mechanism, so that by considering multiple scattering mechanisms, an adjustable parameter corresponding to their relative importance is introduced. This parameter can be adjusted to give the experimentally observed magnitude of the initial slope and the magnitude of σ_a/σ_a^0 at saturation. To give an example of how the calculation for σ_a/σ_a^0 could be used to estimate f, we consider the lamellar compounds of graphite bromine. To fit the experimental data of Sasa[5] two scattering mechanisms were included; $1/\tau_1$ for the $\tau =$ constant mechanism and $1/\tau_2$ for the $N(E_F)\tau =$ constant mechanism, so that $(1/\tau)_{\text{total}} = 1/\tau_1 + 1/\tau_2$. As shown in Fig. 10, a qualitative fit to the experimental data was obtained for $f \sim 0.025$ using $\tau_1^{-1} = 2\tau_2^{-1}(E_F^0)$ at the Fermi level. Of interest is this low value for f and its consistency with another estimate of $f = 0.018 \pm 0.004$ obtained from the analysis of the far-infrared magnetoreflection spectrum in graphite-bromine residue compounds.[23] This agreement should, however, be considered with caution since: (i) the data are for room temperature while the calculation is appropriate to low temperatures, (ii) most of the data are for intercalation concentrations greater than the dilute limit, and (iii) the data for σ_a/σ_a^0 in graphite-bromine published by different workers[4,5] are quite different.

The application of the calculated σ_a/σ_a^0 curves to the alkali-metal intercalation compounds is not as satisfactory as for graphite bromine. Using the results of Fig. 9 (upper abscissa scale), a fit between the calculated and experimental curves is obtained using only the $N(E_F)\tau =$ constant scattering mechanism. The very low value obtained for f ($f \cong 0.05$) is inconsistent with Knight shift,[27] specific heat,[28] and R_H (Ref. 26) measurements which yield $f \sim 1$ for these donor intercalation compounds. Some of this discrepancy may arise because the calculation is appropriate to low temperatures and the experimental data are for room temperature. Furthermore, the applicability of the SWMcC model to dilute alkali-metal intercalation compounds has not been established, as it has been for the graphite-halogen compounds using magnetoreflection techniques[12]; thus, the basic

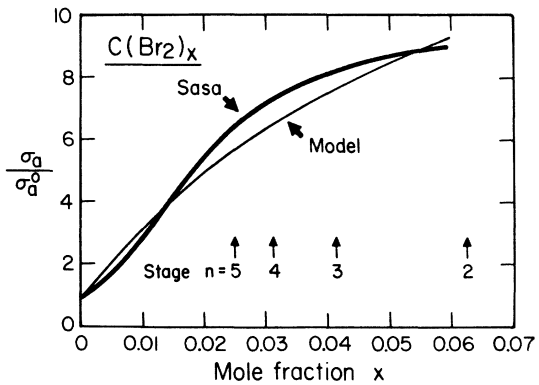

FIG. 10. Light curve gives results for the calculated in-plane electrical conductivity for graphite bromine and the dark curve gives the experimental data of Sasa (Ref. 5). Calculated curve considers a superposition of scattering processes as described in the text. Data are plotted as σ_a/σ_a^0 vs the mole fraction x of Br_2 molecules.

assumptions of the model may not apply to the alkali intercalation compounds. On the basis of these results it would therefore be premature to conclude that carriers in the alkali-metal intercalate monolayers contribute significantly to the in-plane electrical conductivity. Nevertheless, it would be of interest to carry out low temperature σ_a and R_H measurements as a function of intercalate concentration to look for contributions to the electrical conductivity by the intercalate monolayers.

It is of interest to compare the predicted dependence of σ_a on concentration in Fig. 10, which includes the complexity of the 3-dimensional band structure of graphite, with a much simpler version assuming a 2-dimensional effective mass approximation.[29,30] The latter predicts a simple square root dependence, which deviates from the model curve in Fig. 10 by no more than 10% over the concentration range shown. However, the simpler model does not predict the distinctive features in $N(E_F)$ and R_H or the de Haas-van Alphen extremal areas versus concentration which we suggest will be more sensitive observables for the determination of f.

Finally, we discuss the problem of sample characterization in the dilute limit. There is no direct evidence for the existence of well-ordered compounds more dilute than stage 5.[1] For these dilute compounds, the (00l) x-ray reflections are too weak to be observed, so one cannot even confirm the existence of a superlattice along the c axis. Chemical analysis as well as gravimetry simply indicates the absorption of intercalate somewhere within the graphite, which could occupy random sites (for example at defects, as in residue compounds[31]), lamellar interstitial sites, or some combination thereof. Indirect discrimination between the two can be obtained from property measurements sensitive to charged particle scattering (such as σ_a at low temperature) or from the observation of quantum oscillations which require $\omega_c\tau > 1$. Indeed the best evidence for ordered dilute stages comes from the observation of Shubnikov–de Haas periods,[22] resonant Landau level transitions in the magnetoreflection spectra,[12] and insensitivity of the relative intensity of Raman spectra to different preparation techniques in dilute lamellar halogen compounds.[32] In any case, the spirit of the dilute limit model is compatible with either ordered or disordered intercalation since in both cases the graphite portion of the lattice determines the band structure. One would, however, expect differences in f due to the different atomic environments in the residue and lamellar compounds.

ACKNOWLEDGMENTS

The authors would like to thank Dr. K. Nakao, Professor H. Kamimura, Professor W. A. Harrison, and D. D. L. Chung for stimulating discussions. One of us (JEF) is grateful for a NATO Senior Postdoctoral Fellowship which supported him during the initial phase of this work at Cambridge University.

---

*Supported by the NSF Grant No. DMR76-12226.

†Supported by ARPA/AFOSR Contract F44620-75-C-0069.

§Operated under support by the National Science Foundation.

‖The Lincoln Laboratory portion of this work was sponsored by the Department of the Air Force.

[1]G. R. Hennig, Prog. Inorg. Chem. 1, 125 (1959); W. Rüdorff, Adv. Inorg. Chem. 1, 223 (1959); A. R. Ubbelohde and L. A. Lewis, *Graphite and its Crystal Compounds* (Oxford U.P., Oxford, 1960).

[2]A. R. Ubbelohde, Proc. R. Soc. A 327, 289 (1972) (H_2SO_4, Br_2, ICl).

[3]L. C. F. Blackman, J. F. Mathews, and A. R. Ubbelohde, Proc. R. Soc. A 258, 339 (1960) (alkali metals).

[4]A. R. Ubbelohde, Proc. R. Soc. A 309, 297 (1969) (Br_2).

[5]T. Sasa, Y. Takahashi, and T. Mukaibo, Bull. Chem. Soc. Jpn. 43, 34 (1970) (Br_2).

[6]J. J. Murray and A. R. Ubbelohde, Proc. R. Soc. A 312, 371 (1969).

[7]F. R. M. McDonnell, R. C. Pink, and A. R. Ubbelohde, J. Chem. Soc. Part 1, p. 191 (1951).

[8]In previous publications (see Refs. 1–4) f has been referred to as the fractional ionization of the intercalate atom or molecule. This definition suggests that the bonding between carbon and intercalate species is primarily ionic, as assumption which has not been demonstrated experimentally or theoretically and is probably not generally correct for donors and acceptors. Thus, we prefer a more general definition pending elucidation of the nature of the bonding for various intercalate species.

[9]A. R. Ubbelohde, Proc. R. Soc. A 321, 445 (1971).

[10]M. S. Dresselhaus, G. Dresselhaus, and J. E. Fischer, Bull. Am. Phys. Soc. 21, 262 (1976).

[11]Various chemical formulas have been used to describe the molecular unit in the graphite-ICl intercalation compounds [C_{12}ICl in Ref. 2; $C_{8.5}$ICl, $C_{17.0}$ICl, $C_{25.5}$ICl, $C_{34.0}$ICl, $C_{42.5}$ICl in Y. Mizutari, Kyoto Daigaku Genshi Enerugi Kenkyusho Iho, 44, 58 (1973); $C_{5.1-5.4}$ICl in W. Rüdorff, V. Sils, and R. Zeller, Anorg. Allgem. Chem. 283, 299 (1956)]. Since the molecular unit in graphite-ICl has not been established definitively through x-ray measurements, we have selected the molecular unit ICl and the chemical formula C_{12}ICl corresponding to the data points plotted in Ref. 2 from which the curve in Fig. 1 is constructed.

[12]D. D. L. Chung and M. S. Dresselhaus, Solid State Commun. 19, 227 (1976); Physica B (to be published).
[13]J. C. Slonczewski and P. R. Weiss, Phys. Rev. 109, 272 (1958).
[14]J. W. McClure, Phys. Rev. 108, 612 (1957).
[15]I. L. Spain, Phys. Chem. Carbon 8, 1 (1973).
[16]D. E. Nixon and G. S. Parry, J. Phys. Chem. 2, 1932 (1969).
[17]G. R. Hennig, J. Chem. Phys. 20, 1443 (1952).
[18]G. R. Hennig, J. Chem. Phys. 43, 1201 (1965).
[19]W. W. Toy, M. S. Dresselhaus, and G. Dresselhaus, Phys. Rev. B (to be published).
[20]S. Ono and K. Sugihara, J. Phys. Soc. Jpn. 21, 861 (1966).
[21]J. W. McClure, In *Physics of Semimetals and Small-Gap Semiconductors*, edited by D. L. Carter and R. T. Bate (Pergamon, New York, 1971), p. 127.
[22]A. S. Bender and D. A. Young, J. Phys. Chem. 5, 2163 (1972).
[23]D. A. Platts, D. D. L. Chung, and M. S. Dresselhaus, Phys. Rev. B 15, 1087 (1977).
[24]K. Higuchi, H. Suematsu, and S. Tanuma (private communication).
[25]J. M. Ziman, *Electrons and Phonons* (Oxford U.P., Oxford, 1960), Ch. 7.
[26]D. Guérard, G.M. T. Foley, M. Zanini, and J. E. Fischer, Nuovo Cimento (to be published).
[27]G. P. Carver, Phys. Rev. B 7, 2284 (1970).
[28]K. Nakao (private communication); U. Mizutani, T. B. Massalski, and T. Kondow, Phys. Rev. B (to be published).
[29]J. E. Fischer, T. E. Thompson, and F. L. Vogel, ACS Symp. Ser. 21, 418 (1976).
[30]J. E. Fischer, *Carbon* (to be published).
[31]G. R. Hennig, J. Chem. Phys. 20, 1438 (1952).
[32]J. J. Song, D. D. L. Chung, P. C. Eklund, and M. S. Dresselhaus, Solid State Commun. 20, 1111 (1976).